Strangeness production from πN collisions in nuclear matter

K. Tsushima,[1] A. Sibirtsev,[1,2] and A. W. Thomas[1]
[1]*Special Research Center for the Subatomic Structure of Matter and Department of Physics and Mathematical Physics, University of Adelaide, SA 5005, Australia*
[2]*Institut für Theoretische Physik, Universität Giessen, D-35392 Giessen, Germany*
(Received 6 April 2000; published 10 November 2000)

Kaon production in pion-nucleon collisions in nuclear matter is studied in the resonance model. To evaluate the in-medium modification of the reaction amplitude as a function of the baryonic density we introduce relativistic, mean-field potentials for the initial, final, and intermediate mesonic and baryonic states. These vector and scalar potentials were calculated using the quark-meson coupling model. The in-medium kaon production cross sections in pion-nucleon interactions for reaction channels with Λ and Σ hyperons in the final state were calculated at the baryonic densities appropriate to relativistic heavy ion collisions. Contrary to earlier work which has not allowed for the change of the cross section in-medium, we find that the data for kaon production are consistent with a repulsive K^+-nucleus potential.

PACS number(s): 24.10.Jv, 25.40.−h, 25.60.Dz, 25.70.Ef

I. INTRODUCTION

The properties of kaons in nuclear matter have recently attracted enormous interest because of their capacity to signal chiral symmetry restoration or give information on the possibility of kaon condensation in neutron stars [1–4]. Studies with a variety of models [5–8] indicate that the antikaon potential is attractive while the kaons feel a repulsive potential in nuclear matter. The results from kaonic atoms [9,10], as well as an analysis [11–15] of the K^- production from heavy ion collisions [16–20], are in reasonable agreement with the former expectation for antikaons. However, the analysis of available data on K^+ production from heavy ion collisions at SIS energies [18–21] contradicts the predictions that the kaon potential is repulsive. The comparison between the heavy ion calculations and the data [13–15,21,22] indicates that the K^+-meson spectra are best described by neglecting any in-medium modification of the kaon properties. Furthermore, the introduction of even a weakly repulsive K^+-nucleus potential results in a substantial underestimate of the experimental data on kaon production.

Since in heavy ion collisions at SIS energies [16–20] the K^+-mesons are predominantly produced by secondary pions, we investigate the kaon production reactions, $\pi+N\to Y+K$ ($Y=\Lambda,\Sigma$ hyperons), in nuclear matter. To be specific, we combine earlier studies of kaon production in free space with a very successful, relativistic mean-field description of nuclear systems (QMC). All parameters are fixed by earlier studies and the effects of the medium on the reaction cross sections are calculated for the first time. The result is impressive in that the medium effects explain the nuclear production data, without any adjustment of the parameters determined elsewhere, *including* the standard repulsive kaon-nucleus interaction.

Our paper is organized as follows. In Sec. II we introduce the vector and scalar potentials for mesons and baryons involved in the calculations of the $\pi+N\to Y+K$ amplitudes. We explain in Sec. III the resonance model which is used to calculate the cross sections, $\pi+N\to Y+K$. The strangeness production threshold in nuclear matter and its dependence on the baryon density is discussed in Sec. IV. The cross sections of kaon production in $\pi+N$ collisions in vacuum and in nuclear matter at different densities are then evaluated and shown in Sec. V for the $\pi^-+p\to\Lambda+K^0$ reaction and in Sec. VI for the $\pi+N\to\Sigma+K$ reactions. The impact of our results on heavy ion collisions is discussed in Sec. VII. Finally, the summary and conclusions are given in Sec. VIII.

II. MEAN-FIELD POTENTIALS FOR MESONS AND BARYONS

In the present study, we use the quark-meson coupling (QMC) model [23], which has been successfully applied not only to the problems of conventional nuclear physics [24,25] but also to the studies of meson and hyperon properties in a nuclear medium [7,26–35]. A detailed description of the Lagrangian density and the mean-field equations are given in Refs. [7,24–28,31]. The Dirac equations for the quarks and antiquarks in the hadron bags ($q=u,\bar{u},d$ or $\bar{d}$, hereafter), neglecting the Coulomb force, are given by

$$\left[i\gamma\cdot\partial_x-(m_q-V_\sigma^q)\mp\gamma^0\left(V_\omega^q+\frac{1}{2}V_\rho^q\right)\right]\begin{pmatrix}\psi_u(x)\\ \psi_{\bar{u}}(x)\end{pmatrix}=0, \quad (1)$$

$$\left[i\gamma\cdot\partial_x-(m_q-V_\sigma^q)\mp\gamma^0\left(V_\omega^q-\frac{1}{2}V_\rho^q\right)\right]\begin{pmatrix}\psi_d(x)\\ \psi_{\bar{d}}(x)\end{pmatrix}=0, \quad (2)$$

$$[i\gamma\cdot\partial_x-m_s]\psi_s(x)\ \ [\text{or}\ \ \psi_{\bar{s}}(x)]=0. \quad (3)$$

The mean-field potentials for a bag in nuclear matter are defined by $V_\sigma^q=g_\sigma^q\sigma$, $V_\omega^q=g_\omega^q\omega$, and $V_\rho^q=g_\rho^q b$, with g_σ^q, g_ω^q, and g_ρ^q the corresponding quark-meson coupling constants.

The normalized, static solution for the ground state quarks or antiquarks in the hadron, h, may be written as [7,26–28]

$$\psi_f(x)=N_f e^{-i\epsilon_f^* t/R_h^*}\psi_f(\boldsymbol{x}), \quad (4)$$

where f labels the quark flavors, and N_f and $\psi_f(\mathbf{x})$ are the normalization factor and corresponding spin and spatial part of the wave function. The bag radius in medium, R_h^*, which generally depends on the hadron species to which the quarks and antiquarks belong, will be determined through the stability condition for the (in-medium) mass of the meson against the variation of the bag radius [7,24–27,31] [see also Eq. (9)]. The eigenenergies, ϵ_f, in Eq. (4) in units of $1/R_h^*$, are given by

$$\begin{pmatrix} \epsilon_u \\ \epsilon_{\bar{u}} \end{pmatrix} = \Omega_q^* \pm R_h^* \left(V_\omega^q + \frac{1}{2} V_\rho^q \right), \tag{5}$$

$$\begin{pmatrix} \epsilon_d \\ \epsilon_{\bar{d}} \end{pmatrix} = \Omega_q^* \pm R_h^* \left(V_\omega^q - \frac{1}{2} V_\rho^q \right), \tag{6}$$

$$\epsilon_s = \epsilon_{\bar{s}} = \Omega_s, \tag{7}$$

where $\Omega_q^* = \sqrt{x_q^2 + (R_h^* m_q^*)^2}$, with $m_q^* = m_q - g_\sigma^q \sigma$ and $\Omega_s = \sqrt{x_s^2 + (R_h^* m_s)^2}$. The bag eigenfrequencies, x_q and x_s, are determined by the usual, linear boundary condition [24,25]. Note that the lowest eigenenergy for the Dirac equation (Hamiltonian) for the quark, which is positive, can be regarded as the analog of a constituent quark mass.

The hadron masses in symmetric nuclear matter relevant for the present study are calculated by

$$m_h^* = \frac{(n_q + n_{\bar{q}})\Omega_q^* + (n_s + n_{\bar{s}})\Omega_s - z_h}{R_h^*} + \frac{4}{3}\pi R_h^{*3} B, \tag{8}$$

$$\left. \frac{\partial m_h^*}{\partial R_h} \right|_{R_h = R_h^*} = 0. \tag{9}$$

In Eq. (8), n_q ($n_{\bar{q}}$) and n_s ($n_{\bar{s}}$) are the lowest mode light quark (antiquark) and strange (antistrange) quark numbers in the hadron h, respectively, and the z_h parametrize the sum of the center-of-mass and gluon fluctuation effects, and are assumed to be independent of density. The parameters are determined in free space to reproduce their physical masses.

In this study we chose the values $m_q = 5$ MeV and $m_s = 250$ MeV for the current quark masses, and $R_N = 0.8$ fm for the bag radius of the nucleon in free space. Other input parameters and some of the quantities calculated are given in Refs. [24–28]. We stress that while the model has a number of parameters, only three of them, g_σ^q, g_ω^q, and g_ρ^q, are adjusted to fit nuclear data—namely the saturation energy and density of symmetric nuclear matter and the bulk symmetry energy. None of the results for nuclear properties depend strongly on the choice of the other parameters—for example, the relatively weak dependence of the final results for the properties of finite nuclei, on the chosen values of the current quark mass and bag radius, is shown explicitly in Refs. [24,25]. Exactly the same coupling constants, g_σ^q, g_ω^q, and g_ρ^q, are used for the light quarks in the mesons and hyperons as in the nucleon. However, in studies of the kaon system, we found that it was phenomenologically necessary to increase the strength of the vector coupling to the nonstrange quarks in the K^+ (by a factor of 1.4^2) in order to reproduce the empirically extracted K^+-nucleus interaction [6–8,36,37], which is slightly repulsive if one wants to be consistent with the K^+N scattering length, and the corresponding value at $\rho_B = 0.16$ fm^{-3} is estimated to be about 20 MeV [37]. Thus we will use the stronger vector potential, $1.4^2 V_\omega^q$, for the K^+ meson in this study. Calculated mean-field potential felt by K^+ meson, using $1.4^2 V_\omega^q$, is shown in Fig. 2. Through Eqs. (1)–(9) and usual QMC formalism [7,24–28,31] we self-consistently calculate effective masses m_h^* and mean-field potentials $V_{\sigma,\omega,\rho}^q$ in symmetric nuclear matter. The scalar (U_s^h) and vector (U_v^h) potentials felt by the hadrons h in nuclear matter are given by

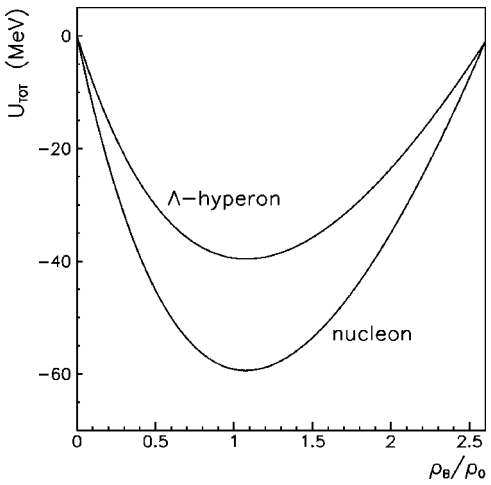

FIG. 1. Total potential U_{tot} for nucleon and Λ hyperon shown as a function of the baryon density ρ_B in units of the nuclear matter saturation density, $\rho_0 = 0.15$ fm^{-3}.

$$U_s^h \equiv U_s = m_h^* - m_h, \tag{10}$$

$$U_v^h = (n_q - n_{\bar{q}}) V_\omega^q - I_3 V_\rho^q, (V_\omega^q \to 1.4^2 V_\omega^q \quad \text{for } K^+). \tag{11}$$

In Eq. (11), I_3 is the third component of isospin projection of the hadron h and the ρ meson mean-field potential V_ρ^q is zero in symmetric nuclear matter. Then, within the approximation that the mean-field potentials are independent of momentum, the four-momentum of the hadron is modified by $p_h^\mu = (\sqrt{\mathbf{p}^2 + m_h^{*2}} + U_v^h, \mathbf{p})$, which modifies not only the kinematical factors such as the flux and the phase space, but also modifies the reaction amplitudes. Obviously, the reaction thresholds are modified in nuclear matter and now depend on the baryon density.

Figure 1 shows the total (U_{tot}) nucleon and Λ-hyperon potentials at zero momenta as function of the baryon density, in units of the saturation density of nuclear matter $\rho_0 = 0.15$ fm^{-3}. Let us recall that at momentum $\mathbf{p} = 0$,

$$U_{tot} = U_s + U_v, \tag{12}$$

and the total potential for the Σ hyperon is almost equal to that for the Λ hyperon.

Figure 1 indicates that both nucleon and hyperon potentials approach minima around normal nuclear matter density,

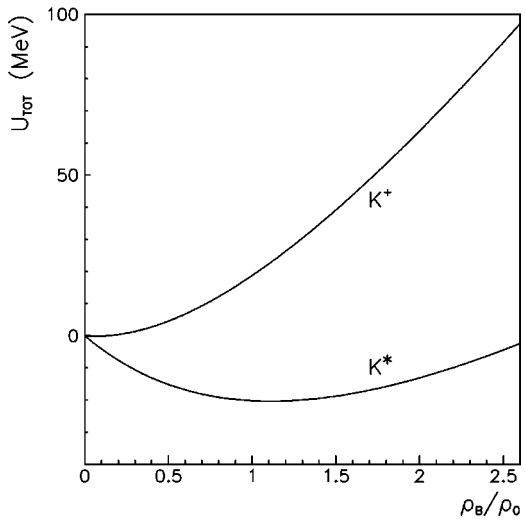

FIG. 2. Total potential U_{tot} for K^+ and $K^*(892)^+$ mesons plotted as a function of the baryon density ρ_B in units of saturation density, $\rho_0 = 0.15$ fm^{-3} of the nuclear matter.

which reflects the fact that around ρ_0 the energy density of nuclear matter is minimized. Figure 2 shows the density dependence of the total K and K^*-meson potentials at zero momenta. The total kaon potential is repulsive as explained before, and depends substantially on the baryon density. The K^*-meson total potential is attractive at baryon densities below $\simeq 2.7\rho_0$.

Now, we will discuss the in-medium modification of the resonance masses. At present it seems that there is no reliable estimate for the in-medium modification of masses for the higher mass baryon resonances. In view of its numerous successful applications elsewhere, we base our estimate on the QMC model [34,35].

We assume that the light quarks in the baryon resonances are responsible for the mass modification in nuclear medium, as in the QMC model [34,35]. However, there is a possibility that the excited state light quarks may couple differently to the scalar σ field from those in the ground states, although we expect the difference is small. Thus we estimate the range for the in-medium baryon resonance masses by the following two extreme cases, i.e., (i) all light quarks including those in the excited states play the same role for the mass modification as those in the ground states, (ii) only the ground state light quarks play the role. These two cases are expected to give the maximum and minimum limits for the mass modifications of the baryon resonances. Specifically, the range for the effective masses of the baryon resonance in medium is given (see, e.g., Ref. [38] for the quark model basis of the baryon resonances):

$$m_{N(1650)} - \delta m_N^* \leqslant m^*_{N(1650)} \leqslant m_{N(1650)} - \frac{2}{3}\delta m_N^*, \quad (13)$$

$$m_{N(1710)} - \delta m_N^* \leqslant m^*_{N(1710)} \leqslant m_{N(1710)} - \frac{1}{3}\delta m_N^*, \quad (14)$$

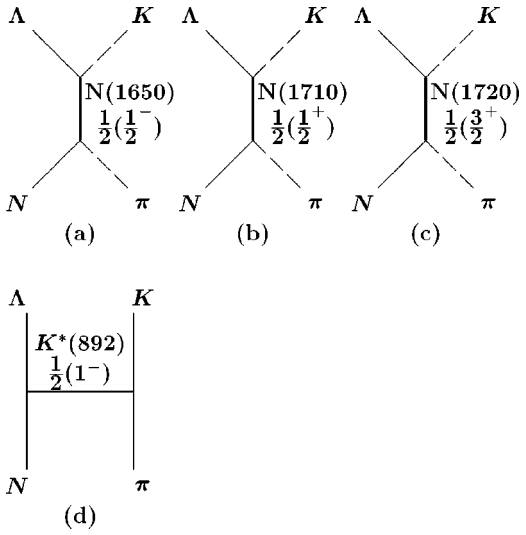

FIG. 3. K and Λ production processes.

$$m_{N(1720)} - \delta m_N^* \leqslant m^*_{N(1720)} \leqslant m_{N(1720)} - \frac{1}{3}\delta m_N^*, \quad (15)$$

$$m_{\Delta(1920)} - \delta m_N^* \leqslant m^*_{\Delta(1920)} \leqslant m_{\Delta(1920)} - \frac{1}{3}\delta m_N^*, \quad (16)$$

$$\text{with} \quad \delta m_N^* = m_N - m_N^*. \quad (17)$$

These in-medium resonance masses may be expected to modify the resonance propagators in the reaction amplitudes. To avoid introducing extra unknown parameters in this initial study, we approximate the in-medium resonance widths appearing in the propagator by the free space ones. From Eqs. (13)–(17) we will show results for the cross section calculated using the lower limit for the resonance masses. However, we have also performed the calculation using the upper limit for the resonance masses, and confirmed that our conclusion remains the same.

III. RESONANCE MODEL

We explain in this section the resonance model [40–43,45–47], which could describe the energy dependence of the total cross sections, $\pi N \to YK$, quite well, and has been used widely in kaon production simulation codes [12–14,22,37,48]. We extend the model by including medium modification of the hadron properties, not only in the kinematic factors such as the flux and the phase space, but also in the reaction amplitudes.

We consider kaon and hyperon production processes in πN collisions shown in Figs. 3 and 4. Because different intermediate states and final states contribute to the $\pi N \to \Lambda K$ and $\pi N \to \Sigma K$ reactions, the in-medium modification of the reaction amplitudes is also expected to be different, as will indeed be shown later.

In Table I we summarize the data for the resonances which are included in the model.

The effective Lagrangian densities used for evaluating the processes shown in Figs. 3 and 4 are

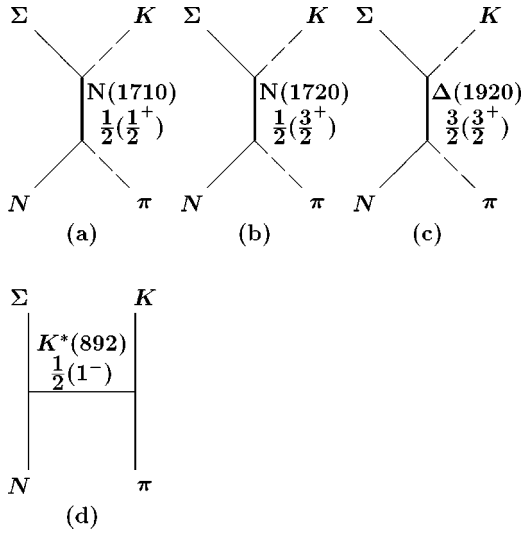

FIG. 4. K and Σ production processes.

$$\mathcal{L}_{\pi NN} = -ig_{\pi NN}\overline{N}\gamma_5\vec{\tau}N\cdot\vec{\pi}, \tag{18}$$

$$\mathcal{L}_{\pi NN(1650)} = -g_{\pi NN(1650)}[\overline{N}(1650)\vec{\tau}N\cdot\vec{\pi} + \overline{N}\vec{\tau}N(1650)\cdot\vec{\pi}], \tag{19}$$

$$\mathcal{L}_{\pi NN(1710)} = -ig_{\pi NN(1710)}[\overline{N}(1710)\gamma_5\vec{\tau}N\cdot\vec{\pi} + \overline{N}\gamma_5\vec{\tau}N(1710)\cdot\vec{\pi}], \tag{20}$$

$$\mathcal{L}_{\pi NN(1720)} = \frac{g_{\pi NN(1720)}}{m_\pi}[\overline{N}^\mu(1720)\vec{\tau}N\cdot\partial_\mu\vec{\pi} + \overline{N}\vec{\tau}N^\mu(1720)\cdot\partial_\mu\vec{\pi}], \tag{21}$$

$$\mathcal{L}_{\pi N\Delta(1920)} = \frac{g_{\pi N\Delta(1920)}}{m_\pi}[\overline{\Delta}^\mu(1920)\vec{\mathcal{I}}N\cdot\partial_\mu\vec{\pi} + \overline{N}\vec{\mathcal{I}}^\dagger\Delta^\mu(1920)\cdot\partial_\mu\vec{\pi}], \tag{22}$$

$$\mathcal{L}_{K\Lambda N(1650)} = -g_{K\Lambda N(1650)}[\overline{N}(1650)\Lambda K + \overline{K\Lambda}N(1650)], \tag{23}$$

$$\mathcal{L}_{K\Lambda N(1710)} = -ig_{K\Lambda N(1710)}[\overline{N}(1710)\gamma_5\Lambda K + \overline{K\Lambda}\gamma_5 N(1710)], \tag{24}$$

$$\mathcal{L}_{K\Lambda N(1720)} = \frac{g_{K\Lambda N(1720)}}{m_K}[\overline{N}^\mu(1720)\Lambda\partial_\mu K + (\partial_\mu\overline{K})\overline{\Lambda}N^\mu(1720)], \tag{25}$$

$$\mathcal{L}_{K\Sigma N(1710)} = -ig_{K\Sigma N(1710)}[\overline{N}(1710)\gamma_5\vec{\tau}\cdot\vec{\Sigma}K + \overline{K}\vec{\Sigma}\cdot\vec{\tau}\gamma_5 N(1710)], \tag{26}$$

$$\mathcal{L}_{K\Sigma N(1720)} = \frac{g_{K\Sigma N(1720)}}{m_K}[\overline{N}^\mu(1720)\vec{\tau}\cdot\vec{\Sigma}\partial_\mu K + (\partial_\mu\overline{K})\vec{\Sigma}\cdot\vec{\tau}N^\mu(1720)], \tag{27}$$

$$\mathcal{L}_{K\Sigma\Delta(1920)} = \frac{g_{K\Sigma\Delta(1920)}}{m_K}[\overline{\Delta}^\mu(1920)\vec{\mathcal{I}}\cdot\vec{\Sigma}\partial_\mu K + (\partial_\mu\overline{K})\vec{\Sigma}\cdot\vec{\mathcal{I}}^\dagger\Delta^\mu(1920)], \tag{28}$$

$$\mathcal{L}_{K^*(892)K\pi} = ig_{K^*(892)K\pi}[\overline{K}\vec{\tau}K^*_\mu(892)\cdot\partial^\mu\vec{\phi} - (\partial^\mu\overline{K})\vec{\tau}K^*_\mu(892)\cdot\vec{\phi}] + \text{H.c.}, \tag{29}$$

TABLE I. Resonances included in the model. Confidence levels of the resonances are $N(1650)$****, $N(1710)$***, $N(1720)$****, and $\Delta(1920)$*** [44]. Note that the $\Delta(1920)$ resonance is treated as an effective resonance which effectively represents the contributions of six resonances, $\Delta(1900)$, $\Delta(1905)$, $\Delta(1910)$, $\Delta(1920)$, $\Delta(1930)$, and $\Delta(1940)$. See Refs. [40,42] for this effective treatment of the $\Delta(1920)$.

Resonance	Width	Channel	Branching ratio	Used
$N(1650)(\frac{1}{2}^-)$	150	$N\pi$	0.60 – 0.80	0.700
	(MeV)	ΛK	0.03 – 0.11	0.070
$N(1710)(\frac{1}{2}^+)$	100	$N\pi$	0.10 – 0.20	0.150
	(MeV)	ΛK	0.05 – 0.25	0.150
		ΣK	0.02 – 0.10	0.060
$N(1720)(\frac{3}{2}^+)$	150	$N\pi$	0.10 – 0.20	0.150
	(MeV)	ΛK	0.03 – 0.10	0.065
		ΣK	0.02 – 0.05	0.035
$\Delta(1920)(\frac{3}{2}^+)$	200	$N\pi$	0.05 – 0.20	0.125
	(MeV)	ΣK	0.01 – 0.03	0.020
$K^*(892)(1^-)$	50	$K\pi$	$\sim$ 1.00	1.00
	(MeV)			

$$\mathcal{L}_{K^*(892)\Lambda N} = -g_{K^*(892)\Lambda N}[\bar{N}\gamma^\mu \Lambda K^*_\mu(892) + \text{H.c.}], \tag{30}$$

$$\mathcal{L}_{K^*(892)\Sigma N} = -g_{K^*(892)\Sigma N}[\bar{N}\gamma^\mu \vec{\tau}\cdot\vec{\Sigma} K^*_\mu(892) + \text{H.c.}]. \tag{31}$$

In the above, the operators $\vec{\mathcal{I}}$ and $\vec{\mathcal{K}}$ are defined by

$$\vec{\mathcal{I}}_{M\mu} \equiv \sum_{l=\pm 1,0} \left(1 l \frac{1}{2}\mu \middle| \frac{3}{2} M\right) \hat{e}^*_l, \tag{32}$$

$$\vec{\mathcal{K}}_{MM'} \equiv \sum_{l=\pm 1,0} \left(1 l \frac{3}{2} M' \middle| \frac{3}{2} M\right) \hat{e}^*_l, \tag{33}$$

with M, μ, and M' being the third components of the isospin projections, and $\vec{\tau}$ the Pauli matrices. N,$N(1710)$,$N(1720)$, and $\Delta(1920)$ stand for the fields of the nucleon and the corresponding baryon resonances. They are expressed by $\bar{N} = (\bar{p},\bar{n})$, similarly for the nucleon resonances, and $\bar{\Delta}(1920) = [\bar{\Delta}(1920)^{++},\bar{\Delta}(1920)^{+},\bar{\Delta}(1920)^{0},\bar{\Delta}(1920)^{-}]$ in isospin space. The physical representations of the kaon field are, $K^T = (K^+,K^0)$ and $\bar{K} = (K^-,\bar{K}^0)$, respectively, and similarly for the $K^*(892)$, where the superscript T means the transposition operation. They are defined as annihilating (creating) the physical particle (antiparticle) states. For the propagators $iS_F(p)$ of the spin 1/2 and $iG^{\mu\nu}(p)$ of the spin 3/2 resonances we use

$$iS_F(p) = i\frac{\gamma\cdot p + m}{p^2 - m^2 + im\Gamma^{full}}, \tag{34}$$

$$iG^{\mu\nu}(p) = i\frac{-P^{\mu\nu}(p)}{p^2 - m^2 + im\Gamma^{full}}, \tag{35}$$

with

$$P^{\mu\nu}(p) = -(\gamma\cdot p + m)\left[g^{\mu\nu} - \frac{1}{3}\gamma^\mu\gamma^\nu - \frac{1}{3m}(\gamma^\mu p^\nu - \gamma^\nu p^\mu) - \frac{2}{3m^2}p^\mu p^\nu\right], \tag{36}$$

where m and Γ^{full} stand for the mass and full decay width of the corresponding resonances. For the form factors, $F(\vec{q})$ ($\vec{q}$ is the momentum of meson, π or K), appearing in the meson-baryon-(baryon resonance) vertices, we use

$$F(\vec{q}) = \left(\frac{\Lambda^2}{\Lambda^2 + \vec{q}^2}\right). \tag{37}$$

For the $K^*(892)$-K-π vertex we adopt the form factor of Ref. [39]:

TABLE II. Values for coupling constants, cutoffs, C and β parameters used in the present study. For details about the coupling constants relevant for $\Delta(1920)$, $g_{\pi N\Delta(1920)}$, and $g_{K\Sigma\Delta(1920)}$, see Refs. [40,42].

Vertex	$g^2/4\pi$	Cutoff Λ (MeV)
πNN	14.4	1050
$\pi NN(1650)$	1.12×10^{-1}	800
$\pi NN(1710)$	2.05×10^{-1}	800
$\pi NN(1720)$	4.13×10^{-3}	800
$\pi N\Delta(1920)$	1.13×10^{-1}	500
$K\Lambda N(1650)$	5.10×10^{-2}	800
$K\Lambda N(1710)$	3.78	800
$K\Lambda N(1720)$	3.12×10^{-1}	800
$K\Sigma N(1710)$	4.66	800
$K\Sigma N(1720)$	2.99×10^{-1}	800
$K\Sigma\Delta(1920)$	3.08×10^{-1}	500
$K^*(892)\Lambda N$	1.62×10^{-2}	1200
$K^*(892)\Sigma N$	1.62×10^{-2}	1200
$K^*(892)K\pi$	5.48×10^{-2}	$C = 2.72$ fm $\beta = 8.88\times10^{-3}$ fm^2

$$F_{K^*(892)K\pi}\left(\left|\frac{1}{2}(\vec{p}_K - \vec{p}_\pi)\right|\right) = C\left|\frac{1}{2}(\vec{p}_K - \vec{p}_\pi)\right| \exp\left(-\beta\left|\frac{1}{2}(\vec{p}_K - \vec{p}_\pi)\right|^2\right). \tag{38}$$

In the calculation, the form factors of Eqs. (37) and (38) are multiplied by the corresponding coupling constants.

The parameters of the model, namely the form factors in the interaction vertices and the coupling constants, were fixed by available experimental data on the different $\pi + N \to Y + K$ reaction channels. Furthermore, the same parameters which were determined by the $\pi + N \to Y + K$ reactions were used in the calculations of strangeness production in baryon-baryon collisions, and they also reproduced the available data reasonably well [45–47]. In Table II we list all values for the coupling constants, cutoffs, C and β parameters relevant for the present study.

Since the strength of the ΛK and ΣK coupling to the various baryonic resonances are different (see Table I), the dynamics of Λ and Σ production are also different. This can be understood as follows.

The amplitude of the resonance propagator in the reaction amplitude, $\pi N \to YK$, becomes maximal when the invariant collision energy crosses the mass of the resonance. Furthermore, the cross section $\sigma(\pi N \to YK)$ is proportional to $(q_Y)^{2l+1}$ near threshold (with l and $q_Y = |\vec{q}_Y|$ the orbital angular momentum and momentum of the YK pair in the center of mass system). In seeking to understand the difference in the behavior of $\sigma(\pi N \to \Lambda K)$ and $\sigma(\pi N \to \Sigma K)$ it is important to note that the former receives a large contribution from the s-wave $N(1650)$ (with $l = 0$), while the latter is dominated by p-wave resonances (with $l = 1$). The subtle inter-

play between the change in momentum dependence associated with threshold variations and the change in resonance amplitudes associated with varying resonance masses is responsible for the different behavior of $\sigma(\pi N\to\Lambda K)$ and $\sigma(\pi N\to\Sigma K)$.

The total free mass of the ΣK system, $m_\Sigma+m_K$, is very close to the mass of the $P_{11}(1710)$ resonance, i.e., $M_{P_{11}}-m_\Sigma-m_K\simeq 27$ MeV, which dictates its substantial role in Σ hyperon production [47]. The situation is different for the ΛK system, since the nearest baryonic resonance is $S_{11}(1650)$ and $M_{S_{11}}-m_\Lambda-m_K\simeq 41$ MeV. Furthermore, because $S_{11}(1650)$ and $P_{11}(1710)$ have different couplings to the final states, ΛK (relative s wave) and ΣK (relative p wave), respectively, the change in the vertices, $S_{11}(1650)\Lambda K$ and $P_{11}(1710)\Sigma K$ due to the momentum modified in medium are also different. Furthermore, when threshold changes as the baryon desnsity varies, the change in the strength of the contributions from the $S_{11}(1650)$ to the $\pi N\to\Lambda K$ reaction and that of the $P_{33}(1920)$ to the $\pi N\to\Sigma K$ reaction should be different as a function of baryonic density. Thus, combining these effects for the $\pi N\to\Lambda K$ and $\pi N\to\Sigma K$ reactions, we can see that the energy dependence of the cross sections in a nuclear medium can be significantly modified.

IV. THE $\pi+N\to Y+K^+$ REACTION THRESHOLD IN NUCLEAR MATTER

The dispersion relation in nuclear matter relating the total energy E and the momentum $\boldsymbol{p}$ of the particle is written as

$$E=\sqrt{\boldsymbol{p}^2+(m+U_s)^2}+U_v\,, \tag{39}$$

where m is the bare mass and U_s, U_v denote the scalar and vector parts of the potential in nuclear matter. The threshold $\sqrt{s_{th}}$ for the reaction $\pi+N\to Y+K^+$ is given as the sum of the total energies of the final K^+ meson and Y hyperon, taking their momenta to be zero and hence

$$\sqrt{s_{th}}=m^K+m^Y+U_s^K+U_s^Y+U_v^K+U_v^Y\,, \tag{40}$$

where now the upper indices denote kaons and hyperons. The solid lines in Fig. 5 show the $K^+\Lambda$ and $K^+\Sigma$ reaction thresholds $\sqrt{s_{th}}$ as a function of the baryon density. Obviously, in free space the scalar and vector potential vanish and the reaction threshold equals to the sum of the bare masses of the produced particles, which is shown by the dashed lines in Fig. 5 for the $K^+\Lambda$ and $K^+\Sigma$ final states.

It is important, that while the K^+-meson energy at zero momentum increases with the baryon density (see Fig. 2), because of the negative Λ and Σ potentials the reaction threshold in nuclear matter at $\rho_B<1.4\rho_0$ is shifted below that in free space.

The maximal downward shift of the reaction threshold in nuclear matter occurs at baryon densities around $\rho_B\simeq 0.6\rho_0$. This value is the result of competition between the simple, linear dependence on density of the vector potentials and the more complicated, nonlinear behavior of the scalar potentials. (A similar competition leads to the saturation of the binding energy of normal nuclear matter in the QMC model.) Furthermore, the maximum of the downward shift of the $\pi+N\to Y+K^+$ reaction threshold amounts to roughly 30 MeV. We also found that at baryon densities $\rho_B>0.2$ fm^{-3} the strangeness production threshold in πN collisions is higher than the free space case.

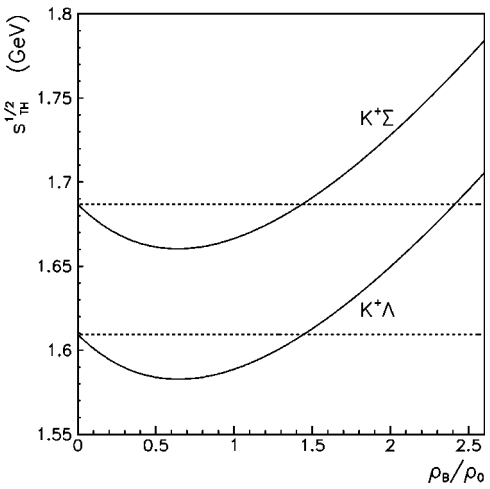

FIG. 5. The threshold energy $\sqrt{s_{th}}$ for $K^+\Lambda$ and $K^+\Sigma$ production given by their total in-medium energy at zero momentum, as a function of the baryon density ρ_B in units of saturation density of nuclear matter, $\rho_0=0.15$ fm^{-3}. The solid lines indicate our results, while the dashed lines show the threshold in free space.

V. THE $\pi+N\to\Lambda+K$ REACTION IN NUCLEAR MATTER

Now we apply the resonance model to calculate the in-medium amplitudes. We keep the coupling constant as well as the form factors at the values found in free space. While this assumption certainly cannot be completely correct in nuclear matter, there are no presently established ways to improve this part of our calculation. In principle, since we started from the reaction amplitude itself, it is possible to include in-medium modifications of the coupling constants as well as the form factors when reliable calculations of the changes of these quantities in nuclear matter become available. In the following calculations we include the vector and scalar potentials for the interacting (initial) nucleons and final kaons and hyperons, as well as for the intermediate baryonic resonances and K^* meson.

Figure 6 shows our results for the differential cross section for the reaction $\pi^-+p\to\Lambda+K^0$ at the invariant collision energy $\sqrt{s}=1683$ MeV. It is calculated both in free space (the solid line) and in nuclear matter, at baryon density $\rho_B=\rho_0$ (the dashed line) and $\rho_B=2\rho_0$ (the dotted line). For comparison, we also show in Fig. 6 the experimental data collected in free space [49,50]. The important finding is that not only the absolute magnitude, but also the shape (the dependence on the $\cos\theta$) of the $\pi^-+p\to\Lambda+K^0$ differential cross section, depends on the baryon density.

One of the simplest ways to construct the in-medium reaction cross section is to take into account only the in-medium modification of the flux and phase space factors while leaving amplitude in matter the same as that in free

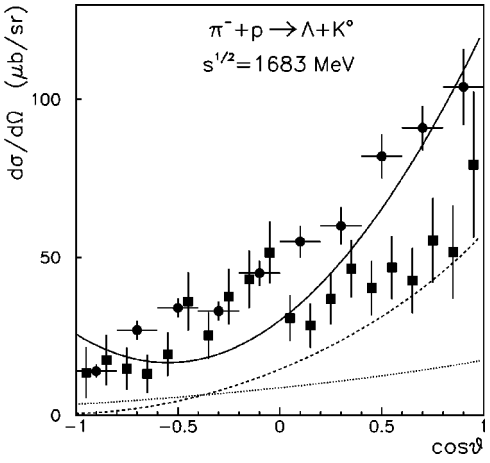

FIG. 6. The $\pi^- + p \rightarrow \Lambda + K^0$ differential cross section at invariant collision energy $\sqrt{s} = 1683$ MeV as a function of the cosine of the kaon emission angle in the center-of-mass system. The experimental data are from Ref. [49] (the squares) and from Ref. [50] (the circles). The lines show our calculations in free space (solid) and in nuclear matter at baryon density $\rho_B = \rho_0$ (dashed) and $\rho_B = 2\rho_0$ (dotted), with $\rho_0 = 0.15$ fm^{-3}.

space, without including medium effect [51]. To shed more light on the problem of how the reaction amplitude itself is modified in nuclear matter, we show in Fig. 7 the dimensionless reaction amplitudes squared for the $\pi^- + p \rightarrow \Lambda + K^0$ reaction, calculated at $\sqrt{s} = 1.7$ GeV and 1.9 GeV, in free space (the solid lines), $\rho_B = \rho_0$ (the dashed lines) and $\rho_B = 2\rho_0$ (the dotted lines). Our calculation clearly indicates that the $\pi^- + p \rightarrow \Lambda + K^0$ reaction amplitude in nuclear matter differs substantially from that in free space at these energies, and that the amplitudes depend on the baryon density.

Finally, the energy dependence of the total $\pi^- + p \rightarrow \Lambda + K^0$ cross section is shown in Fig. 8, as a function of the invariant collision energy, $\sqrt{s}$. The experimental data in free space are taken from Ref. [52]. The calculations for free space are in reasonable agreement with the data, as shown by the solid line. The dashed line in Fig. 8 shows the results obtained for nuclear matter at $\rho_B = \rho_0$, while the dotted line is the calculation at $\rho_B = 2\rho_0$.

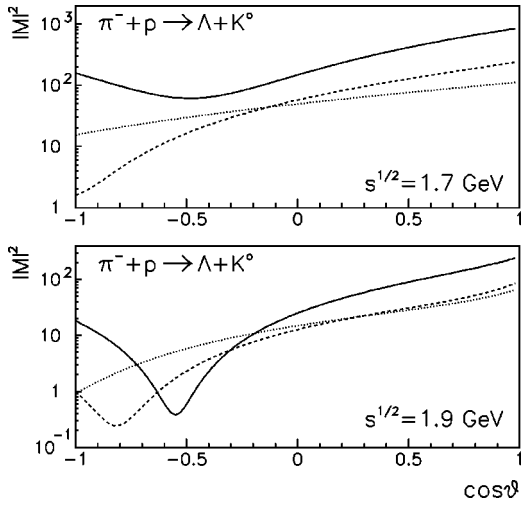

FIG. 7. The (dimensionless) invariant amplitude squared for the $\pi^- + p \rightarrow \Lambda + K^0$ reaction, as a function of $\cos\theta$ (the K^+-meson emission angle in the center-of-mass system), calculated for the invariant collision energies $\sqrt{s} = 1.7$ GeV (upper) and 1.9 GeV (lower). The lines show the result for free space (solid) and for nuclear matter at baryon density $\rho_B = \rho_0$ (dashed) and $\rho_B = 2\rho_0$ (dotted).

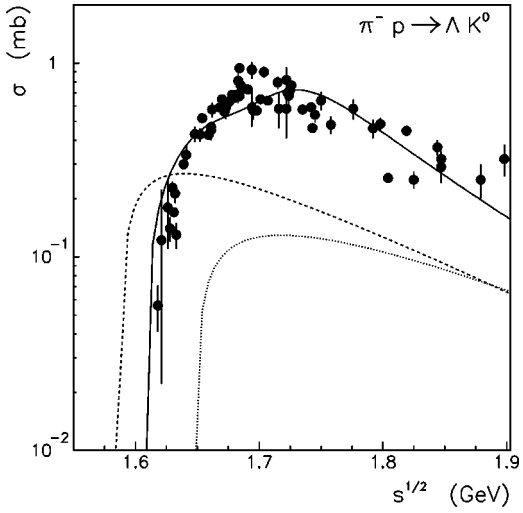

FIG. 8. Energy dependence of the total cross section, $\pi^- + p \rightarrow \Lambda + K^0$, as a function of the invariant collision energy $\sqrt{s}$ calculated for different baryon densities. The data in free space are taken from Ref. [52]. The lines indicate our results for free space (solid) and for nuclear matter at baryon density $\rho_B = \rho_0$ (dashed) and $\rho_B = 2\rho_0$ (dotted). (Only the solid curve should be compared directly with the data.)

Clearly the total $\pi^- + p \rightarrow \Lambda + K^0$ reaction cross section depends substantially on the baryon density. Furthermore, as already discussed in Sec. III, the reaction threshold at baryon density $\rho_B = \rho_0$ is shifted downward as compared to that in free space, while at $\rho_B = 2\rho_0$ it is shifted upwards.

Obviously, heavy ion collisions probe a range of baryon densities from $\rho_B = 0$ up to several times normal nuclear matter density, ρ_0. The calculation of the time and spatial dependence of the baryon density distribution is a vital aspect of dynamical heavy ion simulations. However, a first estimate of the density averaged total $\pi^- + p \rightarrow \Lambda + K^0$ cross section can be gained from Fig. 8. Of course, the data is only available in free space and should only be directly compared with the solid curve. Nevertheless, it is suggestive for the problem of in-medium production to note that a crude average of the in-medium cross sections over the range $0 < \rho_B < 2\rho_0$ would be quite close to the free space cross section at energies around the free space threshold. This seems to provide a reasonable explanation of why the heavy ion calculations including [15,21,22] the $\pi + p \rightarrow \Lambda + K$ cross section in free space, that is without a repulsive kaon potential, can reproduce the data [16–20]. More quantitative calculation and discussion of this effect will be given in Sec. VI.

VI. THE $\pi + N \rightarrow \Sigma + K$ REACTION IN NUCLEAR MATTER

The $\pi + N \rightarrow \Sigma + K$ reaction involves different dynamics in comparison with the $\pi + p \rightarrow \Lambda + K$ reaction, because the

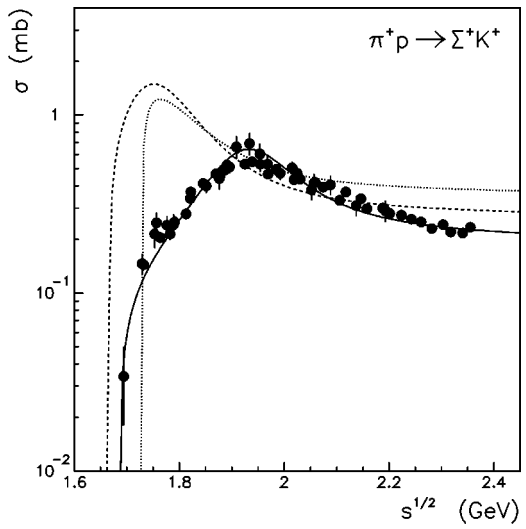

FIG. 9. Energy dependence of the total cross section, $\pi^+ + p \to \Sigma^+ + K^+$, as a function of the invariant collision energy $\sqrt{s}$ calculated for different baryon densities. The data in free space are taken from Ref. [52]. The lines indicate our calculations for free space (solid) and for nuclear matter at baryon density $\rho_B = \rho_0$ (dashed) and $\rho_B = 2\rho_0$ (dotted).

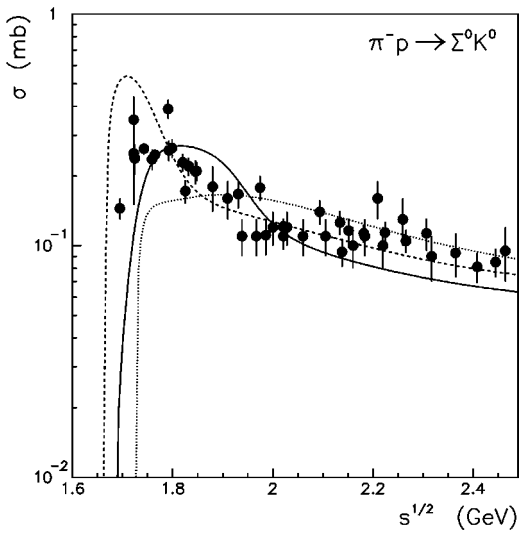

FIG. 10. Energy dependence of the total cross section, $\pi^- + p \to \Sigma^0 + K^0$, as a function of the invariant collision energy $\sqrt{s}$ calculated for different baryon densities. The data in free space are taken from Ref. [52]. The lines indicate our calculations for free space (solid) and for nuclear matter at baryon density $\rho_B = \rho_0$ (dashed) and $\rho_B = 2\rho_0$ (dotted).

reaction involves the different intermediate baryonic resonances. For instance, although the $N(1650)$ resonance couples to ΛN channel, it does not couple to the ΣN state. Moreover, the $\Delta(1920)$ resonance couples to ΣN channel, but does not couple to the ΛN channel in our model. For this reason, the dependence on the baryon density of the reaction in nuclear matter, $\pi + N \to \Sigma + K$, is quite different from that of the $\pi + N \to \Lambda + K$.

In Fig. 9 we show the energy dependence of the total cross section, $\pi^+ + p \to \Sigma^+ + K^+$, as a function of the invariant collision energy $\sqrt{s}$. The experimental data in free space are taken from Ref. [52]. The free space data are well reproduced by the calculations in free space, as shown in Fig. 9 by the solid line. The dashed line indicates the results obtained for nuclear matter at baryon density $\rho_B = \rho_0$, while the dotted line shows the result at $\rho_B = 2\rho_0$.

Again, as already discussed in Sec. III, the density dependence of the hadron masses and the vector potentials leads to a shift of the reaction thresholds in nuclear matter. Because of the density dependence of the Σ-hyperon potential, the threshold at normal nuclear matter density ($\rho_B = \rho_0$) is shifted downwards compared with that in free space. At $\rho_B = 2\rho_0$ the ΣK reaction threshold is shifted upwards relative to the threshold in free space. Moreover, the magnitude of the $\pi^+ + p \to \Sigma^+ + K^+$ cross section depends much more strongly on the density than the $\pi^- + p \to \Lambda + K^0$ reaction.

Figures 10 and 11 show the energy dependence of the total cross sections for the $\pi^- + p \to \Sigma^0 + K^0$ and $\pi^- + p \to \Sigma^- + K^+$ reactions, respectively. The data in free space [52] are well reproduced with the calculations in free space, which are indicated by the solid lines. The cross sections calculated for the nuclear matter, except for $\pi^- + p \to \Sigma^0 + K^0$ at $\rho_B = 2\rho_0$, are substantially enhanced in comparison with those in free space, at energies above near the in-medium reaction thresholds.

VII. IMPACT ON HEAVY ION STUDIES

It is expected that in relativistic heavy ion collisions at SIS energies nuclear matter can be compressed up to baryonic densities of order $\rho_B \simeq 3\rho_0$ [21]. The baryon density ρ_B available in heavy ion collisions evolves with the interaction time t and is given by the dynamics of the heavy ion colli-

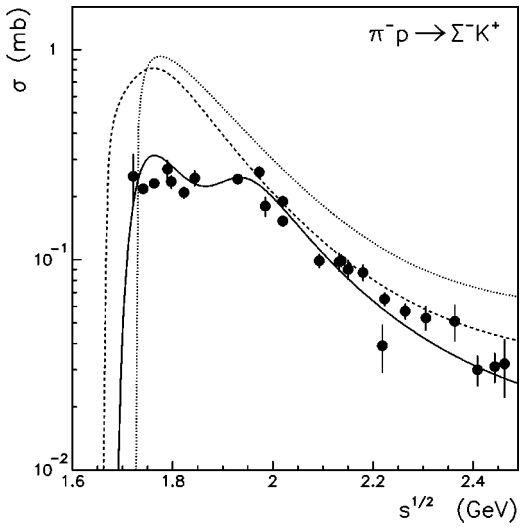

FIG. 11. Energy dependence of the total cross section, $\pi^- + p \to \Sigma^- + K^+$, as a function of the invariant collision energy $\sqrt{s}$ calculated for different baryon densities. The data in free space are taken from Ref. [52]. The lines indicate our calculations for free space (solid) and for nuclear matter at baryon density $\rho_B = \rho_0$ (dashed) and $\rho_B = 2\rho_0$ (dotted).

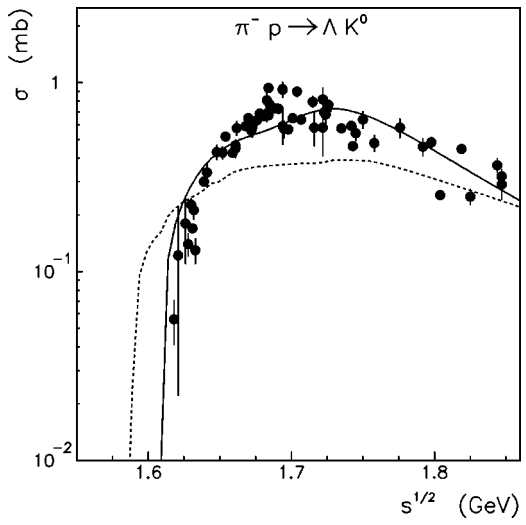

FIG. 12. Energy dependence of the total cross section, $\pi^- + p \rightarrow \Lambda + K^0$, as a function of the invariant collision energy $\sqrt{s}$. The data in free space are taken from Ref. [52]. The solid line indicates our calculation for free space. The dashed line shows the cross section calculated by averaging over the density function profile [53] given by the time evolution obtained for Au+Au collisions at 2*A* GeV [see Eq. (41)].

sion. Moreover, the density is large in the very center of the collision. In the following estimates we investigate the density dependence of the production cross section for central central heavy ion collisions. However, it should be remembered that at the edges, where most particles are expected to be located, the density dependence of the strangeness production mechanism is not strong compared to that of the central zone of the collision.

To calculate the K^+-meson production cross section averaged over the available density distribution we adopt the density profile function obtained by dynamical simulations [53] for Au+Au collisions at 2*A* GeV and at impact parameter $b=0$. This can be parametrized as

$$\rho_B(t) = \rho_{max} \exp\left(\frac{[t-\overline{t}]^2}{\Delta t^2} \right), \tag{41}$$

where the parameters, $\rho_{max}=3\rho_0$, $\overline{t}=13$ fm, and $\Delta t = 6.7$ fm, were fitted to the heavy ion calculations [53].

The total cross section for the $\pi^- + p \rightarrow \Lambda + K^0$ reaction integrated over the time range $5 \leqslant t \leqslant 23$ fm and weighted by the time dependent density profile given in Eq. (41), is shown by the dashed line in Fig. 12. The limits of the t integration were taken from the simulations of the Au+Au collision time evolution in Ref. [53]. The circles and solid line in Fig. 12 show the experimental data in free space [52] and the calculations in free space, respectively.

One can see that the total cross section averaged over the collision time (time dependent density profile) for the $\pi^- + p \rightarrow \Lambda + K^0$ reaction is quite close to the result given in free space integrated up to at energies above the production threshold, up to $\sqrt{s} \simeq 1.7$ GeV. That the results shown in Fig. 12 actually explain why the heavy ion calculations with the free space kaon production cross section might quite reasonably reproduce the experimental data, will be discussed more quantitatively below.

As a matter of fact, the total cross section averaged over the time dependent density profile, shown by the dashed line in Fig. 12, should additionally be averaged over the invariant collision energy distribution available in heavy ion reactions. The number of meson-baryon collisions N_{mB} for the central Au+Au collisions at 2*A* GeV is given in Ref. [54] as a function of the invariant collision energy $\sqrt{s}$. It can be parametrized for $\sqrt{s} > 1$ GeV as

$$\frac{dN_{mB}}{d\sqrt{s}} = N_0 \exp\left(\frac{[\sqrt{s}-\sqrt{s_0}]^2}{[\Delta\sqrt{s}]^2} \right), \tag{42}$$

where the normalization factor $N_0 = 6 \times 10^4$ GeV^{-1}, while $\sqrt{s_0}=1$ GeV and $\Delta\sqrt{s}=0.63$ GeV. Note that at SIS energies N_{mB} is almost entirely given by the pion-nucleon interactions, and heavy meson and baryon collisions contribute only to the high energy tail of the distribution in Eq. (42)—with quite small densities [54]. Finally, if we also average the calculated, in-medium, total cross section for $\pi^- + p \rightarrow \Lambda + K^0$, shown by the dashed line in Fig. 12, over the available energy distribution given in Eq. (42), we obtain an average total kaon production cross section of $\langle K \rangle = 65$ μb for central Au+Au collisions at 2*A* GeV. This result is indeed compatible with the calculations using the free space total cross section of the $\pi^- + p \rightarrow \Lambda + K^0$ reaction, which provide an average total kaon production cross section of $\langle K \rangle = 71$ μb for central Au+Au collisions at 2*A* GeV. Note that the inclusion of even a slight modification of the K^+ mass because of the nuclear medium (without the corresponding changes introduced here) leads to a substantial reduction of the inclusive K^+ spectra (by as much as a factor of 2 or 3), compared to that calculated using the free space properties for the relevant hadrons [14].

We stress that at SIS energies reaction channels with a Σ hyperon in the final state play a minor role, because of the upper limit of the energy available in the collisions. As was illustrated by Fig. 5, the downwardly shifted $\pi + N \rightarrow \Sigma + K$ reaction threshold at small densities is still quite high compared to that for the reaction with the Λ hyperon in the final state.

VIII. SUMMARY

We have calculated the in-medium modification of kaon production in pion-nucleon collisions in nuclear matter using the resonance model developed in Refs. [40–43]. To evaluate the in-medium *K*-meson production for the reaction channels with Λ and Σ hyperons in the final, states, the density dependent potentials for the initial, final and intermediate mesons and baryons (resonances) were introduced to the resonance model amplitudes. The vector and scalar potentials were calculated within the quark-meson coupling model [7,23,26–35]. The $\pi + N \rightarrow \Lambda + K$ and $\pi + N \rightarrow \Sigma + K$ cross sections were calculated for different baryon densities of the nuclear matter. We found that not only are the initial flux and the final phase space of the reactions modified in baryonic

matter, but the reaction amplitudes themselves are also modified.

It was shown, that the total $\pi+N\rightarrow\Lambda+K$ and $\pi+N\rightarrow\Sigma+K$ cross sections depend substantially on the baryonic density. Furthermore, the reaction thresholds and the absolute magnitudes as well as the dependence of the production cross section on the invariant collision energy $\sqrt{s}$ all vary strongly with the density of the nuclear matter.

To evaluate the impact of our microscopic calculations on the heavy ion results, we averaged the kaon production cross section over the baryon density profile, which depends on the evolution time of the heavy ion collision. Furthermore, in order to compare with the experimental data more quantitatively, we calculated the effective total kaon production cross section by averaging over the invariant collision energy distributions available in heavy ion reactions. We found that at low collision energies, the density or time averaged K^+-meson production total cross section, calculated using the in-medium properties for the K^+ meson, hyperons and relevant hadrons, is very close to that calculated using the total cross section given in free space.

Thus our results provide an explanation of why the analyses [13,15,21,22] of available data on K^+ production from heavy ion collisions at SIS energies [18–21] for the K^+ spectra can be reasonably described when one neglects any in-medium modification of the kaon and hadronic properties—i.e., adopting the K^+-meson production cross section given in free space.

In conclusion, our present study shows that if one accounts for the in-medium modification of the production amplitude (i.e., the in-medium properties of the K^+ meson and hadrons) correctly, it is possible to understand K^+ production data in heavy ion collisions at SIS energies, even if the K^+ meson feels the theoretically expected, repulsive mean-field potential. The apparent failure to explain the K^+ production data if one includes the purely kinematic effects of the in-medium modification of the K^+ meson and hadrons appears to be a consequence of the omission of these effects on the reaction amplitudes.

ACKNOWLEDGMENTS

A.S. would like to acknowledge the warm hospitality at the CSSM during his visit. This work was supported by the Australian Research Council and the Forschungszentrum Jülich.

[1] D.B. Kaplan and A.E. Nelson, Phys. Lett. B **175**, 57 (1986); **179**, 409(E) (1986).
[2] G.E. Brown and M. Rho, Phys. Rev. Lett. **66**, 2720 (1991).
[3] C.M. Ko, Z.G. Wu, L.H. Xia, and G.E. Brown, Phys. Rev. Lett. **66**, 2577 (1991); **67**, 1811 (1991).
[4] C.H. Lee, G.E. Brown, D.P. Min, and M. Rho, Nucl. Phys. **A585**, 401 (1995).
[5] T. Waas, M. Rho, and W. Weise, Nucl. Phys. **A617**, 449 (1997).
[6] T. Waas, N. Kaiser, and W. Weise, Phys. Lett. B **365**, 12 (1996); **379**, 34 (1996).
[7] K. Tsushima, K. Saito, A.W. Thomas, and S.V. Wright, Phys. Lett. B **429**, 239 (1998); **436**, 453(E) (1998).
[8] A. Sibirtsev and W. Cassing, Nucl. Phys. **A641**, 476 (1998).
[9] E. Friedman, A. Gal, and C.J. Batty, Phys. Lett. B **308**, 6 (1993); Nucl. Phys. **A579**, 518 (1994).
[10] E. Friedman, A. Gal, and J. Mares, Phys. Rev. C **60**, 024314 (1999).
[11] G.Q. Li, C.M. Ko, and X.S. Fang, Phys. Lett. B **329**, 149 (1994).
[12] W. Cassing, E.L. Bratkovskaya, U. Mosel, S. Teis, and A. Sibirtsev, Nucl. Phys. **A614**, 415 (1997).
[13] G.Q. Li, C.H. Lee, and G.E. Brown, Nucl. Phys. **A625**, 372 (1997).
[14] E.L. Bratkovskaya, W. Cassing, and U. Mosel, Nucl. Phys. **A622**, 593 (1997).
[15] W. Cassing and E.L. Bratkovskaya, Phys. Rep. **308**, 65 (1999).
[16] A. Schroter *et al.*, Z. Phys. A **350**, 101 (1994).
[17] P. Senger *et al.*, Acta Phys. Pol. B **27**, 2993 (1996).
[18] R. Barth *et al.*, Phys. Rev. Lett. **78**, 4007 (1997).
[19] F. Laue *et al.*, Phys. Rev. Lett. **82**, 1640 (1999).
[20] P. Senger and H. Strobele, J. Phys. G **25**, R59 (1999).
[21] P. Senger *et al.*, Prog. Part. Nucl. Phys. **42**, 209 (1999).
[22] G.Q. Li, C.M. Ko, and W.S. Chung, Phys. Rev. C **57**, 434 (1998).
[23] P.A.M. Guichon, Phys. Lett. B **200**, 235 (1989).
[24] P.A.M. Guichon, K. Saito, E. Rodionov, and A.W. Thomas, Nucl. Phys. **A601**, 349 (1996).
[25] K. Saito, K. Tsushima, and A.W. Thomas, Nucl. Phys. **A609**, 339 (1996).
[26] K. Tsushima, D.H. Lu, A.W. Thomas, K. Saito, and R.H. Landau, Phys. Rev. C **59**, 2824 (1999).
[27] A. Sibirtsev, K. Tsushima, and A.W. Thomas, Eur. Phys. J. A **6**, 351 (1999).
[28] K. Tsushima, D.H. Lu, A.W. Thomas, and K. Saito, Phys. Lett. B **443**, 26 (1998).
[29] K. Tsushima, to be published in the ISHEPP XIV proceedings.
[30] K. Tsushima, Nucl. Phys. **A670**, 198c (2000).
[31] K. Saito and A.W. Thomas, Phys. Rev. C **51**, 2757 (1995).
[32] K. Saito, K. Tsushima, and A.W. Thomas, Phys. Rev. C **55**, 2637 (1997).
[33] A.W. Thomas, D.H. Lu, K. Tsushima, A.G. Williams, and K. Saito, to be published in the proceedings of the TJNAF Users Workshop.
[34] K. Tsushima, K. Saito, J. Haidenbauer, and A.W. Thomas, Nucl. Phys. **A630**, 691 (1998).
[35] K. Saito, K. Tsushima, and A.W. Thomas, Phys. Rev. C **55**, 2637 (1997).
[36] T. Waas and W. Weise, Nucl. Phys. **A625**, 287 (1997).
[37] G.Q. Li, nucl-th/9710008, Sec. III B; G.Q. Li, C.-H. Lee, and G.E. Brown, Phys. Rev. Lett. **79**, 5214 (1997).
[38] R.K. Bhaduri, *Models of the Nucleon (From Quarks to Soliton)* (Addison-Wesley, Reading, MA, 1988).
[39] C. Gobbi, F. Iachello, and D. Kusnezov, Phys. Rev. D **50**, 2048 (1994).

[40] K. Tsushima, S.W. Huang, and A. Faessler, Phys. Lett. B **337**, 245 (1994).
[41] K. Tsushima, S.W. Huang, and A. Faessler, J. Phys. G **21**, 33 (1995).
[42] K. Tsushima, S.W. Huang, and A. Faessler, Aust. J. Phys. **50**, 35 (1997).
[43] K. Tsushima, A. Sibirtsev, and A.W. Thomas, Phys. Lett. B **390**, 29 (1997).
[44] Particle Data Group, C. Caso *et al.*, Eur. Phys. J. C **3**, 1 (1998); Particle Data Group, L. Montanet *et al.*, Phys. Rev. D **50**, 1173 (1994); Particle Data Group, K. Hikasa *et al.*, *ibid.* **45**, S1 (1992); Particle Data Group, J. J. Hernandez *et al.*, Phys. Lett. B **239**, 1 (1990).
[45] K. Tsushima, A. Sibirtsev, A.W. Thomas, and G.Q. Li, Phys. Rev. C **59**, 369 (1999); **61**, 029903 (2000).
[46] A. Sibirtsev, K. Tsushima, and A.W. Thomas, Phys. Lett. B **421**, 59 (1998).
[47] A. Sibirtsev, K. Tsushima, W. Cassing, and A.W. Thomas, Nucl. Phys. **A646**, 427 (1999).
[48] G.Q. Li and C.M. Ko, Nucl. Phys. **A594**, 439 (1995); Phys. Rev. C **54**, 1897 (1996); Bao-An Li and Che Ming Ko, *ibid.* **52**, 2037 (1995); Y. Nara *et al.*, Nucl. Phys. **A614**, 433 (1997); C. Fuchs *et al.*, Phys. Rev. C **56**, 606 (1997); Phys. Lett. B **434**, 245 (1998); W.S. Chung, G.Q. Li, and C.M. Ko, Nucl. Phys. **A625**, 347 (1997); W.S. Chung, C.M. Ko, and G.Q. Li, *ibid.* **A641**, 347 (1998); Z.S Wang *et al.*, *ibid.* **A628**, 151 (1998); **A645**, 177 (1999); **A648**, 281 (1999).
[49] T.M. Knasel *et al.*, Phys. Rev. D **11**, 1 (1975).
[50] R.D. Baker *et al.*, Nucl. Phys. **B141**, 29 (1978).
[51] V. Pandharipande and S.C. Pieper, Phys. Rev. C **45**, 791 (1992).
[52] Landolt-Börnstein, New Series, Vol. 8 edited by H. Schopper (1973).
[53] A. Hombach, W. Cassing, S. Teis, and U. Mosel, Eur. Phys. J. A **5**, 77 (1999).
[54] W. Cassing, E.L. Bratkovskaya, and S. Juchem, Nucl. Phys. **A674**, 249 (2000).